frontiers | Frontiers in Energy Research

ORIGINAL RESEARCH
published: 13 July 2022
doi: 10.3389/fenrg.2022.936580

Robust Nonlinear Control of DFIG-Based Wind Farms for Damping Inter-Area Oscillations of Power Systems

Bo Li, Shihai Yang*, Bin Yang and Kaijie Fang

Marketing Service Center, State Grid Jiangsu Electric Power Co., Ltd., Nanjing, China

This article presents a perturbation observer–based robust nonlinear damping control (RNDC) scheme for a doubly fed induction generator (DFIG)–based wind farm to damp the inter-area oscillations of multi-area power systems. In the RNDC scheme, the perturbation term is introduced to describe the combined effects of nonlinearities, uncertainties, and disturbances of multi-area power systems with wind farms. The feedback linearization control is realized for reactive power control loops of the DFIG based on state estimation and perturbation estimation derived from a perturbation observer, thus achieving the damping control of the DFIG. The proposed RNDC scheme only needs one measurement signal, and it does not require any model parameters of the power grid and wind farm. Simulation studies are carried out on a two-area power system model connected with the wind farm to validate the control performance of the RNDC scheme under the conditions of three-phase-to-ground faults, parameter variations, and time delays.

Keywords: DFIG, wind farm, damping control, reactive power control, inter-area oscillations

Edited by:
Dongliang Xiao,
South China University of Technology, China

Reviewed by:
Qi Wang,
Harbin Institute of Technology, China
Weike Mo,
Jinan University, China

****Correspondence:***
Shihai Yang
ysh.young@163.com

Specialty section:
This article was submitted to Smart Grids, a section of the journal Frontiers in Energy Research

Received: *05 May 2022*
Accepted: *25 May 2022*
Published: *13 July 2022*

Citation:
Li B, Yang S, Yang B and Fang K (2022) Robust Nonlinear Control of DFIG-Based Wind Farms for Damping Inter-Area Oscillations of Power Systems. Front. Energy Res. 10:936580. doi: 10.3389/fenrg.2022.936580

1 INTRODUCTION

Wind energy is a cost-effective and environmental-friendly resource, and it has become one of the most promising renewable energy resources to solve the fossil energy crisis and environmental pollution problems (Li et al., 2019; Xiahou K. et al., 2020; Moness and Moustafa, 2020; Xiahou et al., 2021; Xiao et al., 2022). The wind power generation technology has developed rapidly over the past decades. Among various wind power generators, the doubly fed induction generator (DFIG)–based wind turbine (Xue et al., 2019; Xiahou et al., 2018a,b; Wei et al., 2022) has the advantages of high energy conversion efficiency, full active and reactive power control capabilities, and small power converter rating of back-to-back converter. Therefore, the DFIG-based wind turbines have been broadly installed around the world for wind power generation systems, and the DFIG-based wind farms play an important role in the control and operation of power systems.

The modern power system is interconnected by different control areas, and the size of the power system is growing. The inter-area low-frequency oscillation is a threat to the stable operation of the power system, and it has been reported by many countries (Yao et al., 2013; Liu et al., 2022, to be published). With the integration of large-scale wind power, the inter-area oscillation issue becomes more and more severe since the intermittency and volatility of wind power may aggravate the effects of inter-area oscillation and even lead to instability of the power system. Recently, researchers have investigated various damping control methods to mitigate the inter-area oscillations and ensure the stable operation of the power system. Authors have adopted the lead–lag compensator (Yao et al., 2011), networked predictive control (Yao et al., 2015), and dynamic programming control (Zhao et al., 2022, to be published) for designing wide-area damping controllers to suppress the inter-area oscillations of the power system. Nevertheless, the damping controller (Yao et al., 2011, 2015; Zhao et al., 2022, to be published) is only applied for synchronous generators and does not consider the wind farms.

Due to the merits of flexible active and reactive power control ability of the DFIG, recent researchers have used the DFIG-based wind farm to damp the inter-area oscillations of power systems. In the study by Hughes et al., (2006), a classical damping controller is designed for the DFIG to enhance the system dynamic response, and the damping control is similar to the power system stabilizer (PSS) for the synchronous generator. In the study by Miao et al., (2009); Fan et al., (2011), a damping control scheme is designed for the rotor-side converter of the DFIG-based wind farm based on the root locus analysis method so as to improve the damping performance of inter-area oscillations. In the study by Singh et al., (2014); Kunjumuhammed et al., (2017), the classical lead–lag compensator is applied to design the damping controller for the DFIG. The linear robust control method (Yogarathinam and Chaudhuri, 2018) and particle swarm optimization method (Huang and Chung, 2012) are used by researchers for the parameter design of damping controllers of the DFIG.

Nevertheless, the abovementioned linear damping controllers (Hughes et al., 2006; Miao et al., 2009; Fan et al., 2011; Huang and Chung, 2012; Singh et al., 2014; Kunjumuhammed et al., 2017; Yogarathinam and Chaudhuri, 2018) are designed based on the linearized model of the DFIG and power system with respect to one fixed operation point; thus, these damping controllers are weak to model uncertainties and operation point uncertainties. Nonlinear intelligent control methods, such as data-driven, model-free adaptive control (Shi et al., 2020) and adaptive dynamic programming control (Mir and Senroy, 2020), have been applied to design the damping controller for the DFIG, while these controllers are complex and cannot ensure the closed-loop stability of the system. Nonlinear sliding-mode control (SMC)–based damping control (Liao et al., 2016, 2017) has been proposed for the DFIG-based wind farm, and it shows better damping performance than the conventional linear controller. However, the SMC (Liao et al., 2016, 2017) requires many model parameters and measurement signals, which is difficult to be implemented in practice.

This study deals with the aforementioned problems and proposes a perturbation observer–based robust nonlinear damping control (RNDC) scheme for the DFIG-based wind farms to damp the inter-area oscillations of the power system. The nonlinear model of the multi-area power system integrated with the DFIG-based wind farm is built. A perturbation observer is designed based on the input–output linearization model of the nonlinear power system to simultaneously estimate the system state and perturbation state. The nonlinear power system model with the wind farm is regulated by the feedback linearization control based on the state and perturbation estimations provided by the perturbation observer. Simulation studies are carried out on a two-area power system to demonstrate the effectiveness of the proposed RNDC scheme.

This article is organized as follows. **Section 2** depicts the nonlinear model of the two-area power system with the DFIG-based wind farm. **Section 3** illustrates the proposed perturbation observer–based robust nonlinear damping control scheme. Simulation results are given in **Section 4**, and conclusions are drawn in **Section 5**.

2 TWO-AREA POWER SYSTEM MODEL WITH WIND FARM

The configuration of the studied two-area power system is shown in **Figure 1**, in which Area 1 and Area 2 power systems are connected *via* transmission lines, and a wind farm is connected to the Area 1 power system. The wind farm is represented by an equivalent aggregated DFIG-based wind turbine model, which consists of a rotor-side converter (RSC) and grid-side converter (GSC). A damp controller is installed on the DFIG-based wind farm to mitigate the inter-area oscillations between Area 1 and Area 2 power systems.

2.1 Wind Farm Model

The DFIG model (Xiahou and Wu, 2018; Xiahou K. S. et al., 2020) can be expressed in the synchronous rotating d-q reference frame. The stator flux linkages of the DFIG are given as

$$\psi_{\mathrm{sd}} = L_{\mathrm{s}} I_{\mathrm{sd}} + L_{\mathrm{m}} I_{\mathrm{rd}}. \tag{1}$$

$$\psi_{\mathrm{sq}} = L_{\mathrm{s}} I_{\mathrm{sq}} + L_{\mathrm{m}} I_{\mathrm{rq}}. \tag{2}$$

and the rotor flux linkages of the DFIG are represented by

$$\psi_{\mathrm{rq}} = L_{\mathrm{r}} I_{\mathrm{rq}} + L_{\mathrm{m}} I_{\mathrm{sq}}, \tag{3}$$

$$\psi_{\mathrm{rq}} = L_{\mathrm{r}} I_{\mathrm{rq}} + L_{\mathrm{m}} I_{\mathrm{sq}}, \tag{4}$$

where ψ_{sd} and ψ_{sq} are the d-axis and q-axis components of the stator flux, respectively. ψ_{rd} and ψ_{rq} are the d-axis and q-axis components of rotor fluxes, respectively. I_{sd} and I_{sq} are d-axis and q-axis components of stator currents, respectively. I_{rd}

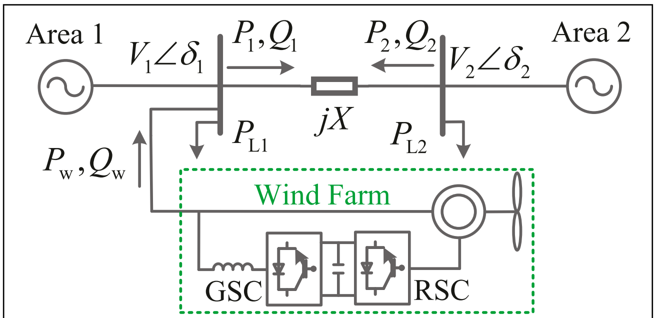

FIGURE 1 | Two-area power system integrated with the DFIG-based wind farm.

and I_{rq} are the d-axis and q-axis components of rotor currents, respectively. L_{ls}, L_{lr}, and L_m are the stator leakage inductance, rotor leakage inductance, and mutual inductance, respectively. $L_s = L_{ls} + L_m$ is the stator self-inductance, and $L_r = L_{lr} + L_m$ is the rotor self-inductance.

The dynamics of stator flux linkages of the DFIG are expressed by

$$\dot{\lambda}_{sd} - \omega_s \lambda_{sq} + R_s I_{sd} - V_{sd} = 0. \tag{5}$$

$$\dot{\lambda}_{sq} + \omega_s \lambda_{sd} + R_s I_{sq} - V_{sq} = 0. \tag{6}$$

and the dynamics of rotor flux linkages are given by

$$\dot{\lambda}_{rd} - \omega_{slip} \lambda_{rq} + R_r I_{rd} - V_{rd} = 0. \tag{7}$$

$$\dot{\lambda}_{rq} + \omega_{slip} \lambda_{rd} + R_r I_{rq} - V_{rq} = 0, \tag{8}$$

where ω_s, ω_r, and $\omega_{slip} = \omega_s - \omega_r$ are the synchronous speed, rotor speed, and slip speed, respectively. V_{sd} and V_{sq} are the d-axis and q-axis components of stator voltages, respectively; V_{rd} and V_{rq} are the d-axis and q-axis components of rotor voltages, respectively; and R_s and R_r are the stator and rotor resistances, respectively.

The stator active and reactive powers of the DFIG are calculated as

$$P_s = -1.5\left(V_{sd} I_{sd} + V_{sq} I_{sq}\right), \tag{9}$$

$$Q_s = -1.5\left(V_{sq} I_{sd} - V_{sd} I_{sq}\right), \tag{10}$$

where P_s is the stator active power and Q_s is the stator reactive power. The speed motion equation of the DFIG can be represented as

$$2H_w \dot{\omega}_r = T_e - T_m - D_w \omega_r, \tag{11}$$

where T_m is the mechanical torque, H_w is the inertia constant, D_w is the damping factor, and T_e is the electromagnetic torque given by

$$T_e = 1.5 L_m \left(I_{sq} I_{rd} - I_{sd} I_{rq}\right). \tag{12}$$

2.2 Power System Model

The two-area power system model integrated with the wind farm illustrated in **Figure 1** is considered, which can be expressed by the swing equation (Kundur, 1994; Tobergte and Curtis, 2013; Xiahou et al., 2022)

$$\begin{cases} \dot{\delta}_{12} = \omega_{12} \\ \dot{\omega}_{12} = \dfrac{P_{m1}}{H_1} - \dfrac{P_{L1}}{H_1} - \dfrac{P_{m2}}{H_2} + \dfrac{P_{L2}}{H_2} \\ \qquad - \dfrac{V_1}{H_1 V_2}\sin\delta_{12} - \dfrac{V_1}{H_2 V_2}\sin\delta_{12} \end{cases} \tag{13}$$

where $\delta_{12} = \delta_1 - \delta_2$ is the rotor angle deviation between Area 1 and Area 2 and δ_1 and δ_2 are the rotor angles of Area 1 and Area 2, respectively. $\omega_{12} = \omega_1 - \omega_2$ is the generator speed deviation between Area 1 and Area 2, and ω_1 and ω_2 are the generator speed of Area 1 and Area 2, respectively. H_1 and H_2 are the equivalent inertia of Area 1 and Area 2, respectively. P_{m1} and P_{m2} are the mechanical power of Area 1 and Area 2, respectively. P_{L1} and P_{L2} are the load power of Area 1 and Area 2, respectively. V_1 and V_2 are the terminal voltage of Area 1 and Area 2, respectively.

The DFIG-based wind farm is connected to Area 1; thus, the two-area power system model with the wind farm becomes

$$\begin{aligned} \dot{\omega}_{12} = & \frac{P_{m1}}{H_1} + \frac{P_w}{H_1} - \frac{P_{L1}}{H_1} - \frac{P_{m2}}{H_2} + \frac{P_{L2}}{H_2} \\ & - \frac{V_1}{H_1 V_2}\sin\delta_{12} - \frac{V_1}{H_2 V_2}\sin\delta_{12} \end{aligned}, \tag{14}$$

where P_w is the active power of the wind farm. A supplementary reactive power controller is adopted to damp the inter-area oscillations of the power system. The reactive power Q_1 of Area 1 can be expressed as

$$\begin{cases} Q_1 = Q_w + Q_c \\ Q_1 = \dfrac{V_2^2 - V_1 V_2 \cos\delta_{12}}{X} \end{cases} \tag{15}$$

where Q_w is the reactive power of the wind farm, Q_c is the reactive power of the capacitive compensator and synchronous generator, and X is the impedance of the transmission line.

3 PERTURBATION OBSERVER–BASED ROBUST NONLINEAR DAMPING CONTROL

3.1 Nonlinear System Model for Damping Control

Taking the power angle $\delta_2 = 0$ as the reference value, it has $\delta_{12} = \delta_1$. Thus, the two-area power system model becomes

$$\begin{cases} \dot{\delta}_1 = \omega_{12} \\ \dot{\omega}_{12} = \dfrac{P_{m1}}{H_1} + \dfrac{P_w}{H_1} - \dfrac{P_{L1}}{H_1} - \dfrac{P_{m2}}{H_2} + \dfrac{P_{L2}}{H_2} \\ \qquad - \dfrac{V_1}{H_1 V_2}\sin\delta_1 - \dfrac{V_1}{H_2 V_2}\sin\delta_1 \end{cases} \tag{16}$$

From **(15)**, the terminal voltage V_1 of the Area 1 power system can be expressed as

$$V_1 = \frac{V_2^2 - Q_w X - Q_c X}{V_2 \cos\delta_1}. \tag{17}$$

Replacing V_1 with **(17)** in **(16)**, it has

$$\begin{cases} \dot{\delta}_1 = \omega_{12} \\ \dot{\omega}_{12} = \dfrac{P_{\text{m1}}}{H_1} + \dfrac{P_{\text{w}}}{H_1} - \dfrac{P_{\text{L1}}}{H_1} - \dfrac{P_{\text{m2}}}{H_2} + \dfrac{P_{\text{L2}}}{H_2} \\ \qquad - \dfrac{\left(V_2^2 - Q_{\text{w}}X - Q_{\text{c}}X\right)\sin\delta_1}{H_1 V_2^2 \cos\delta_1} \\ \qquad - \dfrac{\left(V_2^2 - Q_{\text{w}}X - Q_{\text{c}}X\right)\sin\delta_1}{H_2 V_2^2 \cos\delta_1}. \end{cases} \tag{18}$$

The reactive power control loop of the DFIG can be approximated by a first-order model as

$$Q_{\text{w}} = \frac{Q_{\text{w}}^*}{T_{\text{w}}s + 1}, \tag{19}$$

where Q_{w}^* is the reference value of the reactive power Q_{w} generated from the DFIG-based wind farm. Thus, the damping control model of reactive power loops can be expressed as

$$\Delta Q_{\text{w}} = \frac{\Delta Q_{\text{w}}^*}{T_{\text{w}}s + 1}, \tag{20}$$

where ΔQ_{w} is the reactive power output caused by the damping controller and ΔQ_{w}^* is the damping control input. Based on the abovementioned analysis, the whole system dynamic equation can be written as

$$\begin{cases} \dot{\delta}_1 = \omega_{12} \\ \dot{\omega}_{12} = \dfrac{P_{\text{m1}}}{H_1} + \dfrac{P_{\text{w}}}{H_1} - \dfrac{P_{\text{L1}}}{H_1} - \dfrac{P_{\text{m2}}}{H_2} + \dfrac{P_{\text{L2}}}{H_2} \\ \qquad - \dfrac{\left(V_2^2 - \Delta Q_{\text{w}} - Q_{\text{w}}X - Q_{\text{c}}X\right)\sin\delta_1}{H_1 V_2^2 \cos\delta_1} \\ \qquad - \dfrac{\left(V_2^2 - \Delta Q_{\text{w}} - Q_{\text{w}}X - Q_{\text{c}}X\right)\sin\delta_1}{H_2 V_2^2 \cos\delta_1} \\ \Delta\dot{Q}_{\text{w}} = \dfrac{u - \Delta Q_{\text{w}}}{T_{\text{w}}} \end{cases} \tag{21}$$

where $u = \Delta Q_{\text{w}}^*$ is the control input of the damping controller.

3.2 Controller Design

Taking $x = [x_1, x_2, x_3]^\top = [\delta_1, \omega_{12}, \Delta Q_{\text{w}}]^\top$ as the state vector, the power system model (21) can be expressed as the following nonlinear system model

$$\dot{x} = f(x) + g(x)u, \tag{22}$$

where $g(x) = [0, 0, 1/T_{\text{w}}]^\top$, $f(x) = [f_1(x), f_2(x), f_3(x)]^\top$, $f_1(x) = x_2$, $f_3(x) = -T_{\text{w}}^{-1}x_3$, and

$$\begin{aligned} f_2(x) = {} & \frac{P_{\text{m1}}}{H_1} + \frac{P_{\text{w}}}{H_1} - \frac{P_{\text{L1}}}{H_1} - \frac{P_{\text{m2}}}{H_2} + \frac{P_{\text{L2}}}{H_2} \\ & - \left(\frac{1}{H_1} + \frac{1}{H_2}\right) \frac{V_2^2 - x_3 - Q_{\text{w}}X - Q_{\text{c}}X}{V_2^2} \frac{\sin x_1}{\cos x_1}. \end{aligned} \tag{23}$$

Taking the control target $y = x_2 = \omega_{12}$ as the output signal, the measurement equation is given as

$$y = h(x) = x_2. \tag{24}$$

The input–output linearization method is applied for the single-input-single-output (SISO) nonlinear system model (22)–(24). Differentiating the output variable y until the control signal u explicitly appears, which can be represented by

$$\ddot{y} = \mathcal{L}_f^2 h(x) + \mathcal{L}_g \mathcal{L}_f h(x) \cdot u, \tag{25}$$

where the Lie derivations $\mathcal{L}_f^2 h(x)$, $\mathcal{L}_g \mathcal{L}_f h(x)$ are calculated as

$$\begin{aligned} \mathcal{L}_f^2 h(x) = {} & -\left(\frac{1}{H_1} + \frac{1}{H_2}\right) \frac{\left(V_2^2 - x_3 - Q_{\text{w}}X - Q_{\text{c}}X\right)x_2}{V_2^2 \cos^2 x_1} \\ & -\left(\frac{1}{H_1} + \frac{1}{H_2}\right) \frac{x_3 \sin x_1}{V_2^2 T_{\text{w}} \cos x_1} \end{aligned}. \tag{26}$$

$$\mathcal{L}_g \mathcal{L}_f h(x) = \left(\frac{1}{H_1} + \frac{1}{H_2}\right) \frac{\sin x_1}{V_2^2 T_{\text{w}} \cos x_1}. \tag{27}$$

Since the Lie derivative $\mathcal{L}_g \mathcal{L}_f h(x) \neq 0$, the relative degree of y is obtained as $r = 2$.

The perturbation term ψ of the damping control system is introduced as

$$\psi(x, u, t) = \mathcal{L}_f^2 h(x) + \left(\mathcal{L}_g \mathcal{L}_f h(x) - b_0\right)u \tag{28}$$

to represent the combined effects of nonlinearities, uncertainties, and external disturbances of the system, where the constant parameter b_0 is to be tuned. Based on the definition of the perturbation term in **Eq. 28**, the system model (25) can be transformed as

$$\ddot{y} = \psi(x, u, t) + b_0 u. \tag{29}$$

The new state variable $\xi = [\xi_1, \xi_2]^\top$ is defined to represent the system state of **Eq. 29**, where $\xi_1 = y$ and $\xi_2 = \dot{y}$. Meanwhile, the extended state is defined as $\xi_3 = \psi$ to represent the perturbation term. Therefore, the nonlinear system model (29) can be represented with the third-order state-space form as

$$\Theta : \begin{cases} \dot{\xi}_1 = A\xi + B\left(\xi_3 + b_0 u\right) \\ \dot{\xi}_3 = \dot{\psi}(\cdot) \\ y = C\xi \end{cases} \tag{30}$$

with

$$A = \begin{bmatrix} 0 & 1 \\ 0 & 0 \end{bmatrix}, B = \begin{bmatrix} 0 \\ 1 \end{bmatrix}, C = \begin{bmatrix} 1 & 0 \end{bmatrix}. \tag{31}$$

With the feedback linearization control law

$$u = \frac{-\xi_3 - K\xi}{b_0}, \tag{32}$$

the nonlinear system Θ can be linearized exactly into the following linear system

$$\dot{\xi} = (A - BK)\xi, \tag{33}$$

where K is the feedback gain matrix which is to be designed.

However, the perturbation state ξ_3 of control law (32) is unknown, which is almost impossible to be implemented. Thus, the perturbation observer is designed to estimate the system perturbation state. Based on **Eq. 30**, a perturbation observer $\hat{\Theta}$ is designed for the nonlinear system Θ as follows

$$\hat{\Theta}: \begin{cases} \dot{\hat{\xi}} = A\hat{\xi} + B\left(\hat{\xi}_3 + b_0 u\right) + L\left(y - C\hat{\xi}\right) \\ \dot{\hat{\xi}}_3 = l_3\left(y - C\hat{\xi}\right) \end{cases}, \tag{34}$$

where $\hat{\xi} = [\hat{\xi}_1, \hat{\xi}_2]^\top$ is the estimated value of the system state ξ, $\hat{\xi}_3$ is the estimated value of the perturbation state ξ_3, $L = [l_1, l_2]^\top$, l_3 are observer gains, which are selected as $l_j = \alpha_j \varepsilon^{-j} (j = 1, 2, 3)$, where α_j is chosen such that all the roots of $s^3 + \alpha_1 s^2 + \alpha_2 s + \alpha_3$ have negative real parts, and $\varepsilon \in (0, 1]$ is a small gain parameter.

Based on the system state estimation $\hat{\xi}$ and perturbation state estimation $\hat{\xi}_3$ derived from the perturbation observer, the damping control law of the DFIG-based wind farm is given as

$$u = \frac{-\hat{\xi}_3 - K\hat{\xi}}{b_0}, \tag{35}$$

where the perturbation estimation $\hat{\xi}_3$ is adopted to compensate the effects of the perturbation term and the system state estimation $\hat{\xi}$ is used for the output feedback control. The classical linear quadratic regulator (LQR) method is utilized to design the optimal feedback gain matrix K since the relative degree of y is equal to 2, which is less than the nonlinear system order of 3. Thus, the internal dynamics can be obtained as $\dot{x}_1 = x_2 = y = \xi_1$. When $\xi_1 = \xi_2 = 0$, the zero dynamics of the nonlinear system is given as $\dot{x}_1 = 0$, which indicates the internal stability of the nonlinear system model.

Based on the abovementioned analysis, the block diagram of the proposed perturbation observer–based robust nonlinear damping control scheme is illustrated in **Figure 2**. As seen, the PI-based dual-loop vector control scheme is adopted to control the RSC of the DFIG-based wind farm. The rotor currents I_{rd}, I_{rq} of the DFIG is regulated to their reference values I_{rd}^*, I_{rq}^* with the application of PI current controllers with compensation terms Δ_{rd}, Δ_{rq}. Meanwhile, the active power P_s and reactive power Q_s are, respectively, regulated to their reference values P_s^* and Q_s^* by the PI power controllers. Taking the speed deviation as the measured signal $y = \omega_{12}$, the perturbation observer (34) is implemented based on the input–output linearization model to simultaneously estimate the state and perturbation of the system. Based on **Eq. 35**, the state estimation and perturbation estimation of the perturbation observer are used for output feedback control and perturbation compensation, respectively, thus realizing the robust nonlinear damping control of the DFIG-based wind farm. It is noted that the proposed RNDC scheme only requires the measurement signal of speed deviation, and it does not need any model parameters.

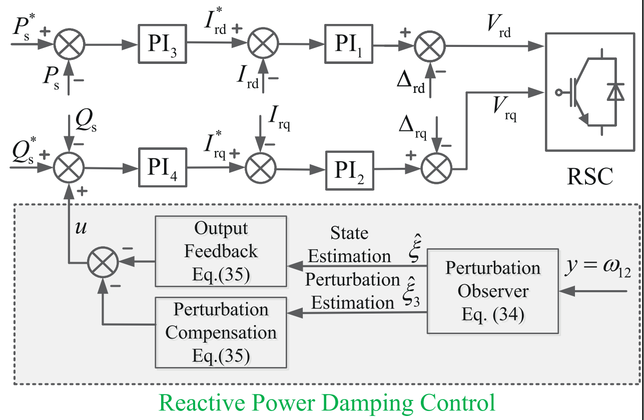

FIGURE 2 | Schematic of the proposed perturbation observer-based RNDC scheme.

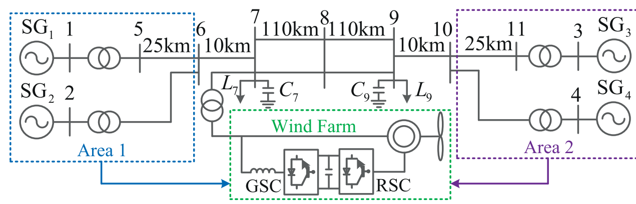

FIGURE 3 | Configuration of the simulated power system.

4 SIMULATION STUDIES

Simulation studies are undertaken on the detailed two-area four-machine power system with the wind farm illustrated in **Figure 3** built in Simulink/Sim Power Systems.

The detailed parameters of the two-area four-machine power system are given in the study by Kundur, (1994). The rated power of Area 1 and Area 2 power is set as 1800 MW;, and the rated power of the DFIG-based wind farm is set as 180 MW; thus, the penetration level of the wind power of Area 1 reached 10%. The parameters of the DFIG-based wind farm are given as follows: rated voltage V_{nom} =690 V, rated frequency f_{nom} =60 Hz, rated power P_{nom} =2 MW, rated wind speed V_{wnom} =11 m/s, stator leakage inductance L_{ls} = 0.18p.u., rotor leakage inductance L_{lr} = 0.16p.u., mutual inductance L_m = 2.9p.u., stator resistance R_s = 0.023p.u., and rotor resistance R_r = 0.016p.u. The proposed RNDC scheme is compared with the classical damping control (CDC) (Miao et al., 2009) and sliding-mode control (SMC) (Liao et al., 2016) schemes under the conditions of three-phase-to-ground faults, parameter variations, and time delays.

4.1 Three-phase-to-ground Fault

In the first case, a three-phase-to-ground short-circuit fault is caused in the middle between Bus 7 and Bus 8 at t =0.5 s, which means the fault location is 110 km away from the Area 1 power system. The simulation results of power angle deviation δ_{12}, speed deviation ω_{12}, active power P_1 of Area 1, active power P_2 of Area 2, active power P_w of wind farm, reactive power Q_w of wind farm, rotor speed ω_r of wind farm, and DC-link voltage V_{dc} of wind farm are given in **Figure 4**.

As seen, after the three-phase-to-ground fault happens, the responses δ_{12} and ω_{12} of the two-area power system present low-frequency oscillations. All the three damping control schemes of the CDC, SMC, and RNDC can damp the inter-area oscillations,

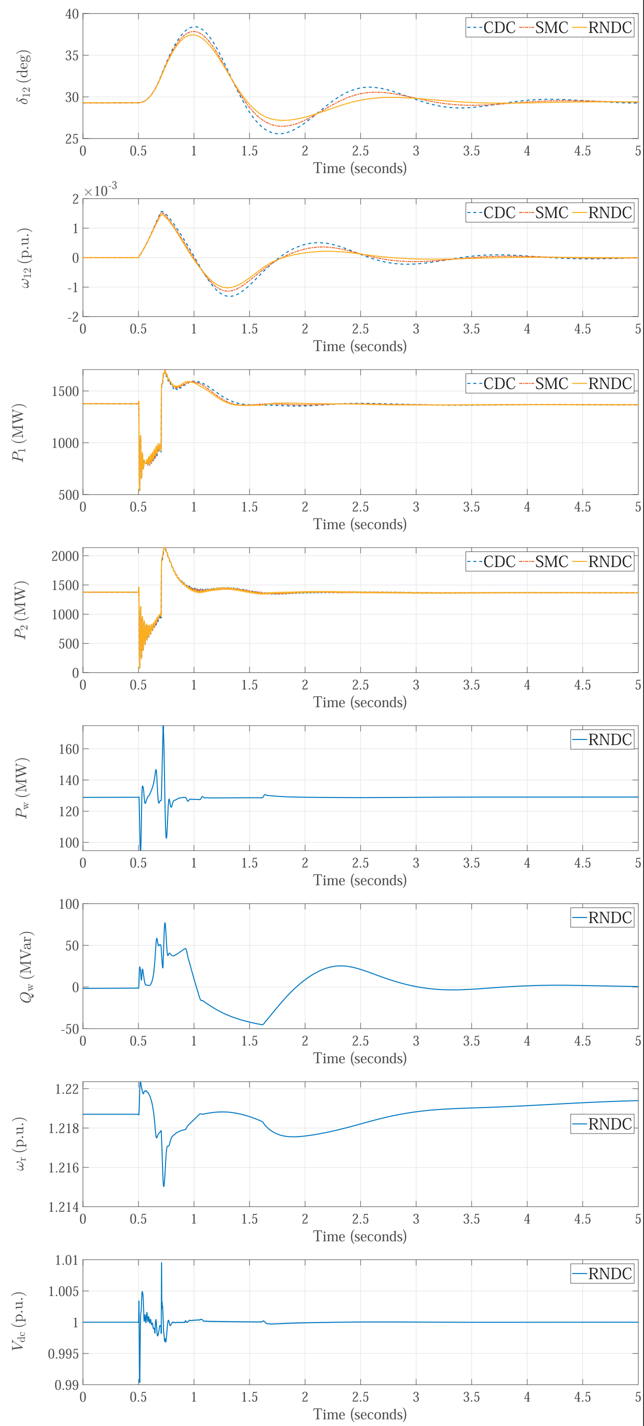

FIGURE 4 | Simulation results obtained in the case where a three-phase-to-ground fault occurs in the middle of the transmission line.

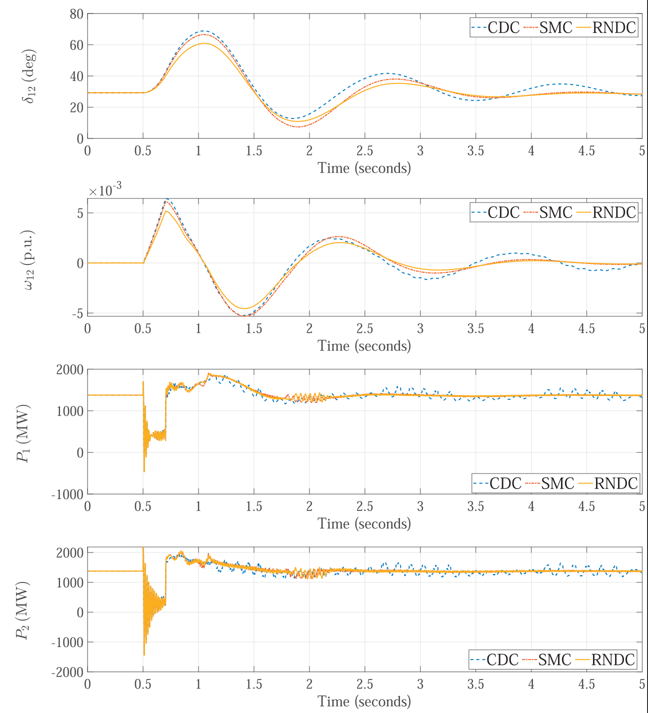

FIGURE 5 | Simulation results obtained in the case where a three-phase-to-ground fault occurs close to the Area 1 power system.

while the proposed RNDC scheme shows better damping performance than both the CDC and SMC. Meanwhile, the RNDC scheme adjusts the reactive power Q_w of the wind farm to damp the oscillations, and the responses of active power P_w, reactive power Q_w, rotor speed ω_r, and DC-link voltage V_{dc} of the wind farm can quickly reach the stable states.

In addition, a three-phase-to-ground short-circuit fault is caused 20 km away from the Area 1 power system, and the simulation results are shown in **Figure 5**. Since the fault location is close to Bus 7, the responses of power angle deviation δ_{12}, speed deviation ω_{12}, active power P_1 of Area 1, and active power P_2 of Area 2 present much larger oscillations than the simulation results in **Figure 4**. According to the simulation results, the proposed RNDC scheme still shows better damping performance than both the CDC and SMC schemes, which verify the effectiveness of the RNDC scheme.

4.2 Parameter Variations

The performance of the proposed RNDC scheme is further compared with that of the SMC scheme under the condition of parameter variations. In this case, the equivalent inertia H_2 of Area 2 and the impedance X of transmission line are varied with +20% and −20% errors, respectively. Meanwhile, a three-phase-to-ground short-circuit fault is caused at the middle between Bus 7 and Bus 8 at t =0.5 s, and the simulation results of the SMC and RNDC are illustrated in **Figures 6A,B**, respectively. As can be seen from the responses of δ_{12}, ω_{12}, P_1, and P_2, the parameter variations deteriorate the control performance of the SMC. This is due to the fact that the implementation of the SMC requires many model parameters of Area 1 and Area 2 power systems. Nevertheless, the implementation of the RNDC does not require any model parameters. The simulation results of the RNDC obtained with and without parameter variations are almost the same, which demonstrates the stronger robustness of the RNDC against parameter uncertainties than the SMC.

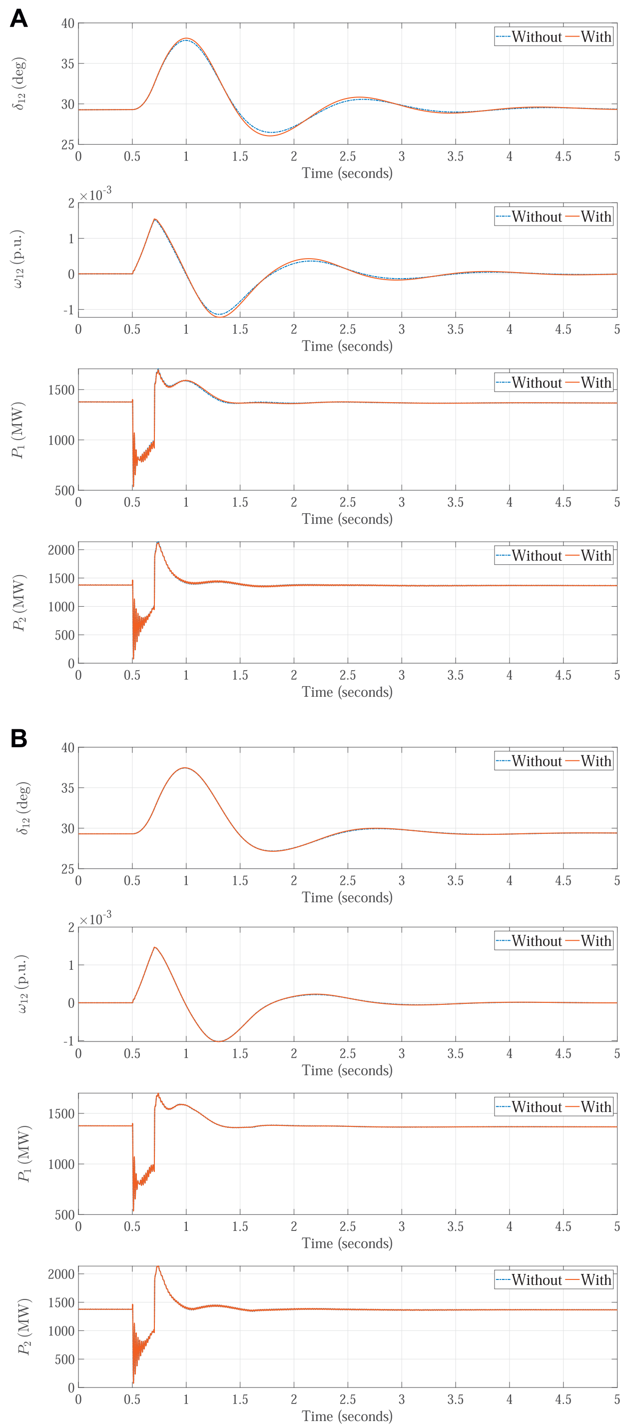

FIGURE 6 | Simulation results of the **(A)** SMC and **(B)** RNDC obtained under parameter variations.

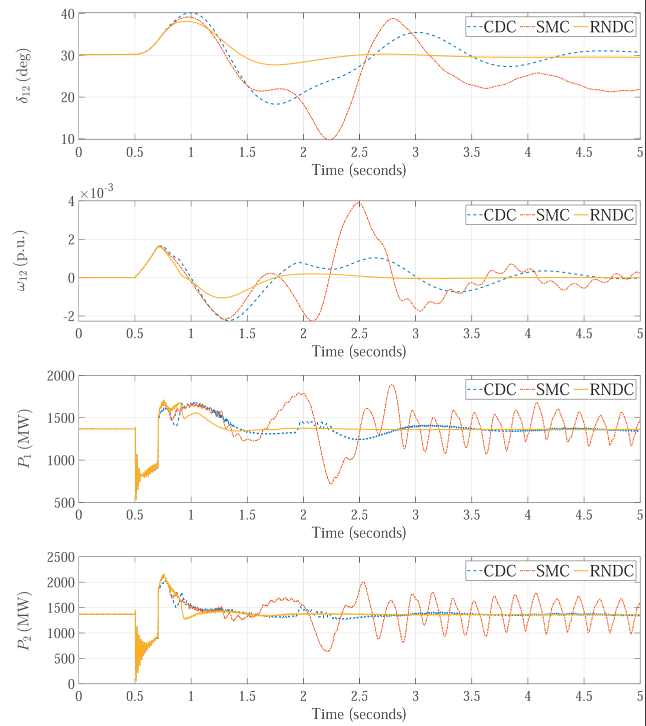

FIGURE 7 | Simulation results obtained under the condition of time delay.

4.3 Time Delays

In this case, the proposed RNDC scheme is tested under the condition of time delay. A time delay of 50 ms is added to the measurement signal derived from the Area 2 power system, a three-phase-to-ground short-circuit fault is caused at the middle between Bus 7 and Bus 8 at t =0.5 s, and the simulation results are shown in **Figure 7**.

As observed from the responses of δ_{12}, ω_{12}, P_1, and P_2, the time delay of the measurement signal degrades the performance of the CDC, SMC, and RNDC schemes. Since the SMC scheme requires many measurement signals from Area 2 power systems, the SMC scheme presents large fluctuations, and the power systems is almost unstable. Both the CDC and RNDC can still damp the inter-area oscillations, and the RNDC shows much better control performance than the CDC, which reveals the strong adaption ability of the RNDC to time delays.

5 CONCLUSION

This study has proposed an RNDC scheme for DFIG-based wind farms to damp the inter-area oscillations of power systems. The RNDC scheme is implemented based on the perturbation observer and feedback linearization control method. Simulation studies are undertaken on a two-area power system model with 10% level penetration of the wind farm. According to the simulation results obtained under the conditions of three-phase-to-ground short-circuit faults, parameter variations, and time delays, conclusions can be drawn as follows.

First, the proposed RNDC scheme can damp the inter-area oscillations of power systems caused by three-phase-to-ground short-circuit faults, and it shows better damping performance than both the CDC scheme and SMC scheme. Meanwhile, the proposed RNDC scheme presents stronger robustness against parameter variations and better adaption ability to time delays.

This is due to the fact that the RNDC scheme only requires one measurement signal and does not need any model parameters. In addition, the accurate perturbation estimation derived from the perturbation observer is applied to compensate the unknown dynamics of nonlinear systems in the RNDC scheme. Finally, with the perturbation compensation and output feedback control, the RNDC can realize the exact feedback linearization control of DFIG-based wind farms and effectively damp the inter-area oscillations of multi-area power systems.

DATA AVAILABILITY STATEMENT

The original contributions presented in the study are included in the article/Supplementary Material; further inquiries can be directed to the corresponding author.

AUTHOR CONTRIBUTIONS

BL: Investigation, methodology, software, and writing—original draft. SY: Supervision, data curation, and writing—review and editing. BY: Visualization and writing—review and editing. KF: Writing—review and editing.

FUNDING

This work was supported by the project of State Grid Jiangsu Electric Power Co., Ltd. (research and economic analysis of cluster control strategy for multi-client adjustable loads, No. J2021152).

REFERENCES

Fan, L., Yin, H., and Miao, Z. (2011). On Active/reactive Power Modulation of Dfig-Based Wind Generation for Interarea Oscillation Damping. *IEEE Trans. Energy Convers.* 26, 513–521. doi:10.1109/tec.2010.2089985

Huang, H., and Chung, C. Y. (2012). Coordinated Damping Control Design for Dfig-Based Wind Generation Considering Power Output Variation. *IEEE Trans. Power Syst.* 27, 1916–1925. doi:10.1109/tpwrs.2012.2190110

Hughes, F. M., Anaya-Lara, O., Jenkins, N., and Strbac, G. (2006). A Power System Stabilizer for Dfig-Based Wind Generation. *IEEE Trans. Power Syst.* 21, 763–772. doi:10.1109/tpwrs.2006.873037

Kundur, P. (1994). *Power System Stability and Control*. New York, NY: Power System Stability and Control.

Kunjumuhammed, L. P., Pal, B. C., Oates, C., and Dyke, K. J. (2017). Electrical Oscillations in Wind Farm Systems: Analysis and Insight Based on Detailed Modeling. *IEEE Trans. Sustain. Energy* 7, 51–62.

Li, P., Xiong, L., Wu, F., Ma, M., and Wang, J. (2019). Sliding Mode Controller Based on Feedback Linearization for Damping of Sub-synchronous Control Interaction in Dfig-Based Wind Power Plants. *Int. J. Electr. Power & Energy Syst.* 107, 239–250. doi:10.1016/j.ijepes.2018.11.020

Liao, K., He, Z., Xu, Y., Chen, G., Dong, Z. Y., and Wong, K. P. (2016). A Sliding Mode Based Damping Control of Dfig for Interarea Power Oscillations. *IEEE Trans. Sustain. Energy* 8, 258–267.

Liao, K., Xu, Y., He, Z., and Dong, Z. Y. (2017). Second-order Sliding Mode Based P-Q Coordinated Modulation of Dfigs against Interarea Oscillations. *IEEE Trans. Power Syst.* 32, 4978–4980. doi:10.1109/tpwrs.2017.2667228

Liu, S., Zenelis, I., Li, Y., Wang, X., Li, Q., and Zhu, L. (2022). Markov Game for Securing Wide-Area Damping Control against False Data Injection Attacks. *IEEE Syst. J.* to be published.

Miao, Z., Fan, L., Osborn, D., and Yuvarajan, S. (2009). Control of Dfig-Based Wind Generation to Improve Interarea Oscillation Damping. *IEEE Trans. Energy Convers.* 24, 415–422. doi:10.1109/tec.2009.2015980

Mir, A. S., and Senroy, N. (2020). DFIG Damping Controller Design Using Robust CKF-Based Adaptive Dynamic Programming. *IEEE Trans. Sustain. Energy* 11, 839–850. doi:10.1109/tste.2019.2910262

Moness, M., and Moustafa, A. M. (2020). Real-time Switched Model Predictive Control for a Cyber-Physical Wind Turbine Emulator. *IEEE Trans. Ind. Inf.* 16, 3807–3817. doi:10.1109/tii.2019.2937549

Shi, X., Cao, Y., Shahidehpour, M., Li, Y., Wu, X., and Li, Z. (2020). Data-driven Wide-Area Model-free Adaptive Damping Control with Communication Delays for Wind Farm. *IEEE Trans. Smart Grid* 11, 5062–5071. doi:10.1109/tsg.2020.3001640

Singh, M., Allen, A. J., Muljadi, E., Gevorgian, V., Zhang, Y., and Santoso, S. (2014). Interarea Oscillation Damping Controls for Wind Power Plants. *IEEE Trans. Sustain. Energy* 6, 967–975.

Tobergte, D. R., and Curtis, S. (2013). *Power System Stability and Control*.

Wei, C., Zhao, Y., Zheng, Y., Xie, L., and Smedley, K. M. (2022). Analysis and Design of a Nonisolated High Step-Down Converter with Coupled Inductor and Zvs Operation. *IEEE Trans. Ind. Electron.* 69, 9007–9018. doi:10.1109/tie.2021.3114721

Xiahou, K., Li, M. S., Liu, Y., and Wu, Q. H. (2018a). Sensor Fault Tolerance Enhancement of Dfig-Wts via Perturbation Observer-Based Dpc and Two-Stage Kalman Filters. *IEEE Trans. Energy Convers.* 33, 483–495. doi:10.1109/tec.2017.2771250

Xiahou, K., Lin, X., Liu, Y., and Wu, Q. H. (2018b). Robust Rotor-Current Sensorless Control of Doubly Fed Induction Generators. *IEEE Trans. Energy Convers.* 33, 897–899. doi:10.1109/tec.2018.2813089

Xiahou, K., Liu, Y., Wang, L., Li, M. S., and Wu, Q. H. (2020b). Switching Fault-Tolerant Control for Dfig-Based Wind Turbines with Rotor and Stator Current Sensor Faults. *IEEE Access* 7, 103390–103403.

Xiahou, K., Liu, Y., and Wu, Q. H. (2022). Decentralized Detection and Mitigation of Multiple False Data Injection Attacks in Multiarea Power Systems. *IEEE J. Emerg. Sel. Top. Ind. Electron.* 3, 101–112. doi:10.1109/jestie.2021.3112919

Xiahou, K. S., Liu, Y., Li, M. S., and Wu, Q. H. (2020a). Sensor Fault-Tolerant Control of Dfig Based Wind Energy Conversion Systems. *Int. J. Electr. Power & Energy Syst.* 117, 105563–105577. doi:10.1016/j.ijepes.2019.105563

Xiahou, K. S., Liu, Y., Zhang, L. L., Li, M. S., and Wu, Q. H. (2021). Robust Current Sensorless Control of Vsc-Based Mtdc Transmissions for Integrating Wind Farms. *IEEE J. Emerg. Sel. Top. Power Electron.* 9, 7383–7394. doi:10.1109/jestpe.2020.3004868

Xiahou, K. S., and Wu, Q. H. (2018). Fault-tolerant Control of Doubly-Fed Induction Generators under Voltage and Current Sensor Faults. *Int. J. Electr. Power & Energy Syst.* 98, 48–61. doi:10.1016/j.ijepes.2017.11.028

Xiao, D., AlAshery, M. K., and Wei, Q. (2022). Optimal Price-Maker Trading Strategy of Wind Power Producer Using Virtual Bidding. *J. Mod. Power Syst. Clean Energy* 10, 766–779. doi:10.35833/mpce.2020.000070

Xue, Z. Y., Xiahou, K. S., Li, M. S., Ji, T. Y., and Wu, Q. H. (2019). Diagnosis of Multiple Open-Circuit Switch Faults Based on Long Short-Term Memory Network for Dfig-Based Wind Turbine Systems. *IEEE J. Emerg. Sel. Top. Power Electron.* 8, 2600–2610.

Yao, W., Jiang, L., Wen, J., Wu, Q., and Cheng, S. (2015). Wide-area Damping Controller for Power System Interarea Oscillations: A Networked Predictive Control Approach. *IEEE Trans. Contr. Syst. Technol.* 23, 27–36. doi:10.1109/tcst.2014.2311852

Yao, W., Jiang, L., Wen, J., Wu, Q. H., and Cheng, S. (2013). Wide-area Damping Controller of Facts Devices for Inter-area Oscillations Considering Communication Time Delays. *IEEE Trans. Power Syst.* 29, 318–329.

Yao, W., Jiang, L., Wu, Q. H., Wen, J. Y., and Cheng, S. J. (2011). Delay-dependent Stability Analysis of the Power System with a Wide-Area Damping Controller Embedded. *IEEE Trans. Power Syst.* 26, 233–240. doi:10.1109/tpwrs.2010.2093031

Yogarathinam, A., and Chaudhuri, N. R. (2018). Wide-area Damping Control Using Multiple Dfig-Based Wind Farms under Stochastic Data Packet Dropouts. *IEEE Trans. Smart Grid* 9, 3383–3393. doi:10.1109/tsg.2016.2631448

Zhao, Y., Yao, W., Nan, J., Fang, J., Ai, X., Wen, J., et al. (2022). Resilient Adaptive Wide-Area Damping Control to Mitigate False Data Injection Attacks. *IEEE Syst. J.* to be published.

Conflict of Interest: Authors BL, SY, BY, and KF were employed by Marketing Service Center, State Grid Jiangsu Electric Power Co., Ltd.

Publisher's Note: All claims expressed in this article are solely those of the authors and do not necessarily represent those of their affiliated organizations, or those of the publisher, the editors, and the reviewers. Any product that may be evaluated in this article, or claim that may be made by its manufacturer, is not guaranteed or endorsed by the publisher.